Reconstruction of Holocene hydroclimatic variability in Subarctic treeline lakes using lake sediment grain-size end-members

Andrew L Macumber

Ottawa-Carleton Geoscience Center and Department of Earth Sciences, Carleton University, 1125 Colonel By Drive, Ottawa, K1S 5B6, Canada*

Email: a.macumber@qub.ac.uk

*School of Natural and Built Environments, Queen's University Belfast, Elmwood Avenue, Belfast, BT7 1NN, United Kingdom.

R Timothy Patterson

Ottawa-Carleton Geoscience Center and Department of Earth Sciences, Carleton University, Canada

Jennifer M Galloway

Geological Survey of Canada/Commission Géologique du Canada – Calgary, Canada

Hendrik Falck

Northwest Territories Geological Survey, Department of Industry, Tourism and Investment, Government of the NWT, Canada

Graeme T Swindles

School of Geography, University of Leeds, United Kingdom

Abstract

Current climate trends are expected to result in the northward expansion of the subarctic treeline leading to changes in vegetation cover and permafrost distribution: as they did during the Holocene Climate Optimum when the treeline was 150 km north of its current position. The impacts of these changes on the region's hydrology are still poorly understood. The grain-size distributions of treeline lake sediments provide an important proxy related to spring melt conditions that can be used to reconstruct hydroclimatic variability. End-member mixing analysis was used to model depositional end-members in fifty-five modern lake sediment samples and two sediment cores spanning the mid to late Holocene collected from above and below the treeline in the central Northwest Territories, Canada. Cold climatic intervals (e.g. Dark Ages Cold Period, Little Ice Age) were characterised by an increase in the very coarse silt and the fine sand end-members. This was interpreted to be a response to degradation of vegetation cover and/or permafrost development. We observed increases in fine and coarse silt end-members during warmer climatic intervals (e.g. Medieval Climate Anomaly) and over the past *c.* 300 yr BP. This pattern is probably the result of extended melt seasons, with greater losses to evaporation and increased infiltration. The most pronounced paleo-hydroclimatological change over the last *c.* 8000 yr BP was the abrupt increase in a very coarse silt end-member (mode = 50-200 μm) at *c.* 6300 yr BP. We interpreted the sedimentological change as an increase in winter precipitation and more energetic spring melt conditions: leading to the spring melt becoming the dominant lacustrine sediment delivery mechanism. These results place modern hydrological changes in a millennial context and show that analysis of temporal changes in the hydroclimatological system can provide insight into the future states of these sensitive subarctic ecosystems.

Keywords

Grain-size analysis, end-member mixing analysis, paleo-hydroclimate reconstruction, paleoclimate, Subarctic, Treeline

Introduction

The boreal forest covers about 17% of the continental area of the Earth and has experienced some of the most rapid recent warming in the Northern Hemisphere (Gauthier et al., 2015). The central Northwest Territories represents an important boreal region for the study of Holocene climate variability due to the association between the northern treeline boundary and the southern boundary of the Arctic Front, which links this region to global climate teleconnections (Moser and MacDonald, 1990). This interface also represents the boundary between continuous and discontinuous permafrost zones (Spence and Woo, 2008), making it a particularly important area to study hydroclimatic variability during treeline migrations. The position of the boreal forest treeline has shifted significantly in the past in response to climate warming associated with the Holocene Climate Optimum and the treeline is expected to shift northward again if current warming continues (MacDonald et al., 1993). The total impact of climate change on the regional hydrology is still poorly understood.

Long-term proxy records of past climate that span previous warm climate intervals are necessary to place recent and future changes into context and provide a baseline to current warming trends (Kokfelt et al., 2009; Mullan et al., 2016; Upiter et al., 2014; Viau and Gajewski, 2009; Walsh et al., 2011). Lakes contain continuous sedimentary archives of biological, chemical and physical proxies of past environmental conditions, influenced by broad-scale patterns of Holocene natural climate variability (Huang et al., 2004; MacDonald et al., 1993, 2009; Moser and MacDonald, 1990; Paul et al., 2010; Pienitz et al., 1999; Rühland and Smol, 2005; Upiter et al., 2014; Wolfe et al., 1996). The grain-size distributions of lake sediments are the product of hydraulic interactions within a lake and its catchment, and thus can be used as a proxy for changes in regional hydrology and global atmospheric circulation (Chen et al., 2004; Cockburn and Lamoureux, 2008a; Conroy et al., 2008; Francus et al., 2002; Kirby et al., 2010; Sun et al., 2002; Xiao et al., 2012). Laser diffraction analysis of lake sediments can create high-resolution proxy time-series (Sperazza et al., 2004) since very little material (i.e. 1 cm^3 wet volume) is required and samples can be processed very quickly (i.e. 8 minutes/sample). Temporal resolution can be further increased through the use of specialised sediment core subsampling equipment (Macumber et al., 2011).

Grain-size distributions are often multimodal and consist of dynamic subpopulations sorted by different sediment production, transport and accumulation processes (Doeglas, 1946; Weltje and Prins, 2007). Some depositional processes can be linked to lake-catchment hydraulic energy and thus reflect climate dependent processes. End-member mixing analysis (EMMA) is a new and promising methodology for extracting end-members from the eigenspace of a dataset based on the principles of factor analysis and principal components analysis (Dietze et al., 2012). EMMA aims to provide a genetic interpretation of grain-size distributions with minimal assumptions (Dietze et al., 2012; Weltje and Prins, 2003, 2007), using all available samples from an archive to un-mix subpopulations (Dietze et al., 2014).

We aim to reconstruct the hydroclimatic variability of the central treeline region of Canada over the last 8000 years by modeling end-members in two Holocene-aged sediment cores collected from lakes above and below the modern treeline in the central Northwest Territories, Canada (Figure 1 & Table 1). Modeled end-members in fifty-five modern lake sediment samples from sites across the treeline region (Figure 1) in combination with physical and chemical characteristics of each lake are used to characterise depositional conditions of modeled end-members. An extended record of hydroclimatic variability, encompassing both past cold and warm periods, will help to translate predictions of climate models into hydrological responses and contextualise modern trends.

[insert Figure 1]

Figure 1. Map of the study area and sites. See Table 1 for lake details. Figure after Crann et al., (2015).

[insert Table 1]

Table 1. Properties of the modern lakes (Figure 1). Shore distance - the distance from the collection site to the nearest shoreline. C:N – the ratio of carbon to nitrogen in lake sediment. DD – decimal degrees. DO – bottom water dissolved oxygen.

Catchment-lake dynamics

Geography and Geomorphology of the Region

Pleistocene glaciation, ending 10,000 – 9,000 years ago, scoured the Canadian Shield to produce a rolling topography of undulating bedrock uplands, soil-mantled slopes and soil-filled valleys that often contain wetlands and lakes (Dyke and Prest, 1987; Spence and Woo, 2008). Soils are poorly developed and are predominantly cryosols characterised by grain-sizes ranging from clay to sand (Smith et al., 2009). The present-day treeline – where forest stands are open and lichen woodlands merge into areas of shrub tundra (Galloway et al., 2010) – runs NW/SE across the study area roughly delineating the position of the polar front (Figure 1; Huang et al., 2004), as well as the transition from discontinuous to continuous permafrost zones (Spence and Woo, 2008).

Danny's Lake is located 40 km southwest of the modern treeline (63.48 N, 112.54 W) (Figure 1; Table 1). It is a small, cold polymictic lake that was well-mixed in March 2010 and August 2012 (Macumber et al., 2012). The lake is surrounded by gently sloping hills with local highs, roughly 20 m above the lake surface, to the northwest and east. Discontinuous permafrost exists in the region (Natural

Resources Canada, 2009). Danny’s lake has two sub-basins: a shallow basin with a gradual slope and a larger northern sub-basin (Appendix A1 Figure 1).

Carleton Lake is located 120 km north of the present-day treeline (64.26 N, 110.10 W) (Figure 1; Table 1). Like Danny’s Lake, Carleton Lake is a small cold polymictic lake that is well-mixed year-round (Macumber et al., 2012). Upslope areas, approximately 20 m above the lake surface, lie near the north and northwest. Lowland areas lie to the east and south. Carleton Lake occurs within an area of continuous permafrost but lies close to extensive discontinuous permafrost (Natural Resources Canada, 2009). Upiter et al., (2014), used variation in chironomid species assemblages in a different core from Carleton Lake to reconstruct July temperature variations for the middle to late Holocene.

Climate of the Region

The present climate of the region is continental, characterised by short summers and long cold winters. Annual precipitation is low (175 – 200 mm) and mean daily January temperatures range from -17.5°C to -27.5°C, while mean daily July temperatures range from 7.5°C to 17.5°C (Natural Resources Canada, 2015b).

Annual snow cover forms in October and lasts until the end of April or beginning of May (Spence and Woo, 2008).

Previous paleoclimate reconstructions have identified three main stages of climate and landscape development during the Holocene. The first stage occurred between *c.* 8500 yr BP and *c.* 6300 yr BP when birch-dominated shrub tundra transitioned to spruce-forest tundra following regional deglaciation (Huang et al., 2004; Sulphur et al., 2016). The second stage was marked by the rapid northward expansion of the treeline by about 50 km relative to its present-day position (Figure 1); owing to the northward movement of the polar front, in response to the decay of the Laurentide Ice Sheet, between *c.* 6300 and 3000 yr BP (Huang et al., 2004; Kaufman et al., 2009; MacDonald et al., 1993; Moser and MacDonald, 1990; Sulphur et al., 2016). The most recent stage began with the onset of the Holocene Neoglacial (*c.* 4300 yr BP) when cooling resulted in the southward retreat of the treeline to its current position (Huang et al., 2004; Sulphur et al., 2016).

Hydroclimatic model of sediment transport

For lakes in the central Northwest Territories the majority of allochthonous material is transported by runoff generated during several days of snowmelt in spring as summer rain events are too low in intensity to exceed infiltration (Cockburn and Lamoureux, 2008a; Francus et al., 2008; Spence and Woo, 2008). The hydraulic energy of spring runoff is modulated by the amount of winter precipitation (i.e. snow pack) and the ambient temperature (Cockburn and Lamoureux, 2008a, 2008b; Spence and Woo, 2008). Cockburn and Lamoureux, (2008a, 2008b) observed that cool snowmelt conditions were characterised by reduced melt energy resulting in less snow cover losses and a larger contributing area that could sustain high discharge for longer (Cockburn and Lamoureux, 2008a). Increased duration of meltwater ponding during cool springs was also associated with more intense runoff as compared to a warmer season with equivalent snowpack (Cockburn and Lamoureux, 2008a). Cool snowmelt conditions can bring coarser sediment to the sample sites due to greater and longer sustained runoff (Cockburn and Lamoureux, 2008b). In contrast, warm spring conditions were characterised by an acceleration of the melt period, greater evaporative and ablative losses and snowpack fragmentation. The fragmented snowpack reduced runoff contribution area, introduced a greater potential for losses due to infiltration into thawed soil and increased flow resistance. As a result, warm spring snowmelts were characterised by low-energy delivery of more uniform finer sediment (10-20 µm) (Cockburn and Lamoureux, 2008b).

Methods

Field

Lake sediment sampling. In August 2012, sediment-water interface sediments of 55 lakes spanning the boreal forest, forest-tundra ecotone and tundra (62.77 N to 65.38 N and from 113.45 W to 109.65 W; Figure 1 and Table 1) were collected using an Ekman grab sampler using a helicopter equipped with floats. We targeted the deepest area of small and shallow (3 – 8 m) lakes using a portable depth sounder (Table 1). The top 5 mm of sediment was collected from the Ekman grab sampler. Due to the low sedimentation rate that exists in these types of lakes (Crann et al., 2015) this could represent deposition spanning the past 30 to 100 years. During collection, water can drain from the Ekman grab potentially carrying away fine grain sediment. The gelatinous texture of the sediment due to the high organic content might partly mitigate this, yet there is still the possibility that fine grain sediment is lost. Lake sediment cores were obtained from Danny's Lake and

Carleton Lake using a freeze corer lowered through the ice during winter (Galloway et al., 2010; Macumber et al., 2012). In March 2010, a 114.5 cm sediment core was collected from Danny's Lake that included the sediment-water interface (Macumber et al., 2012). The coring site at Danny's Lake was located on the northern slope of the larger sub-basin at a depth of four meters (Appendix A1 Figure 1). In March 2012, a 107.4 cm sediment core was collected from Carleton Lake that included the sediment-water interface. Carleton Lake has a single basin (Appendix A1 Figure 1) and the coring site was in the southern end of the basin at a depth of two meters. To maximize temporal resolution both sediment freeze cores were sub-sampled at millimeter-scale intervals using a custom designed sledge microtome (Macumber et al., 2011).

Lake physical parameters (Table 1). We measured the water column dissolved oxygen (%) profile with a portable YSI multi-parameter instrument (Macumber et al., 2012). The lake surface area (m^2), catchment size (m^2) and shore slope (degrees) were calculated using digital elevation models and hydrological shape files available via the GEOGRATIS portal (Natural Resources Canada, 2015a). In addition, we used the GRASS GIS (v7.0) (Foundation, 2015) "r.watershed" package to model catchment size and “r.slope.aspect” package to model catchment slope. Distance from shore was calculated using tools available in Google Earth (v7.1.5.1557).

Laboratory

Grain-size analysis. Grain-size distributions for 94 different grain-size classes, ranging from 0.4 to 2500 μm, were determined for every site and core sub-samples using a Beckman Coulter LS 13 320 Laser Diffraction-Particle Size Analyzer with a Universal Liquid Module using the Fraunhofer model. We pretreated samples for grain-size analysis following a protocol modified from Murray, (2002) and van Hengstum et al., (2007). To oxidize organic matter, samples were placed in a 30% H_2O_2 solution until reactions ceased. A hydrochloric acid treatment was deemed unnecessary since carbonate content was less than 1% dry mass (Griffith and Clark, 2013). Modern lake samples were sent to the G.G. Hatch Stable Isotope Laboratory to measure the isotopic composition of organic carbon and nitrogen, as well as their elemental abundance (Griffith and Clark, 2013).

Age-depth models of sediment cores. We applied a reservoir correction (Abbott and Stafford, 1996; Yu et al., 2007) of 430 years to the Danny's Lake sediment core age-depth model presented by Crann et al., (2015) and Sulphur et al., (2016). We also used the IntCal 13 calibration curve (Reimer et al., 2013). A reservoir correction was used since freeze coring yielded an intact sediment-water interface yet the extrapolation of the age-depth model resulted in a large offset at the top of the core. Bulk sediment can exhibit reservoir effects leading to much older estimates than the true age (Abbott and Stafford, 1996). Patterson et al., (2017) confirmed the presence of lake reservoir effects in the central Northwest Territories. They found an offset of *c.* 200 years between the radiocarbon model estimate and the true age of a visible White River tephra layer. Reservoir effects may vary over time related to hydroclimatic change and thus dates below the colour change (90 cm), interpreted here as a major hydrologic change, are contentious. Above the colour change, independent constraints such as terrestrial macrofossil dates were unavailable but the sedimentology remained relatively consistent and the reservoir effect is assumed to be a systematic error. For the Carleton Lake core five bulk radiocarbon dates were submitted to ^{14}CHRONO Center (Belfast, United Kingdom) for AMS radiocarbon dating. We calibrated all radiocarbon ages using the IntCal13 calibration curve (Reimer et al., 2013) and report the ages in years before present (yr BP). We constructed the Carleton Lake age-depth model using CLAM since the program used to construct the age-depth model for Danny's Lake (i.e., BACON) requires more than five radiocarbon dates. The year when the core was collected (2012) was used as the age of the sediment-water interface with an error of ± 5 years. A smoothing parameter of 0.3 was employed. Radiocarbon ages younger than AD1950 were calibrated in CALIBomb. No offset was present, so no reservoir effect was applied. The table of radiocarbon dates for both cores is found in Appendix 2. For both Danny's and Carleton Lake, we applied a five-sample smoothing average to the modelled deposition time (yr/mm) based on the constructed age-depth models.

EMMA. We performed EMMA separately on each grain-size dataset. We followed the procedure of Dietze et al., (2012) and (2014) using extensions implemented in the R package EMMAgeo (Dietze and Dietze, 2013). See Appendix 3 for full details. Only robust end-members were included, defined as end-members recurring in the majority of model runs with non-overlapping and interpretable grain-size distributions (Dietze et al., 2014).

Constrained ordination of modern lakes end-members. We performed a redundancy analysis (i.e., constrained ordination) to investigate the depositional characteristics of the modern lake robust end-members the 'rda' function in the R package 'vegan' (Oksanen, 2013). We used five environmental parameters to constrain the variance in the modern lake end-members (Table 2). We used a box-cox transformation (Box and Cox, 1964) to reduce observed asymmetry (Osborne, 2010) in the environmental parameters. We used the 'standardize' method in the 'decostand' function of the R Package 'vegan' (Oksanen et al., 2017) to scale the environmental parameters to zero mean and unit variance as they use different units of measurement. We summed the fractional abundances of both sand end-members as they were present in only few sites and most likely are the result of similar depositional conditions. We used a Hellinger transformation to make the end-members suitable for the linear-based method of redundancy analysis (Birks et al., 2012; Rao, 1995). A detailed discussion of data treatment and parameter selection can be found in the supplemental materials (Appendix 4).

Table 2. Environmental parameters used to constrain the modern lake end-members (redundancy analysis). See the methods for how parameters were measured. See Appendix 4 for a detailed discussion of redundancy analysis.

Parameter	Unit	Significance
Distance from shore	meters	Sites close to shore would be more energetic.
Principal component of lake depth and shore slope.	Lake depth (meters) Shore slope (degrees)	Lake depth and shore slope were highly correlated. Reduced to a signal component of variability. Reflects basin and catchment morphology.
Watershed area / Lake area	Ratio	Greater values reflect greater terrestrial inputs and water renewal rates.
Carbon:Nitrogen (C:N)	Ratio	Greater values reflect greater amounts of terrestrial sourced material.
Lake bottom dissolved oxygen	Percent	Low values reflect stratification of the water column.

Results

Stratigraphy

Visual inspection of the Danny's Lake core revealed a distinct colour change at ca. 90 cm from olive (Munsell chart: 2.5y 4/3) to brownish black (2.5y 3/2). There were no other stratigraphic features apparent visually or through X-ray imaging. The Carleton Lake core was a uniform olive black colour (Munsell chart: 5y 2.5/2) and massive in texture as determined both visually and by X-ray imaging. Both cores have water contents in excess of 90% and are thus assumed to have been collected from the accumulation zones (Blais and Kalff, 1995; coring sites illustrated in Appendix A1).

Age-depth models

Age-depth relationships were constructed for both sediment cores (Appendix 2 Figures 1 & 2). The basal date of the Danny's Lake core was *c.* 8052 yr BP. The total chronological error (TCE), the difference between the maximum and minimum age (2 sigma range) at the base of the Danny's Lake core was *c.* 1400 yr BP. There is a decreasing trend in the TCE from the base of the core to 0 cm, and the TCE does not exceed *c.* 200 yr BP from 40 – 0 cm. All ages quoted are median ages. The basal date of the Carleton Lake core was *c.* 3064 yr BP (TCE = *c.* 191 yr BP) while our grain size analysis only covers *c.* 2804 yr BP to present.

End-member mixing analysis (EMMA)

To separate end-member distributions from the mixture of distributions present in the grain-size analysis results we used end-member mixing analysis (EMMA; Appendix 3). Table 3 lists properties of each dataset, as well as input and boundary parameters we used for the EMMA. Figure 2 displays the original multimodal grain-size distributions for each dataset along the top row, which formed the basis for our EMMA. Below these are the grain-size distributions of the modelled robust end-members. Table 4 lists physical attributes and the variance explained by each robust end-member. The robustness of the modeled end-members can be assessed based on the size of their standard deviations (Dietze et al., 2014). For example, the coarse silt end-member in Danny's Lake is much more robust than the coarse silt end-member for the modern lakes (Figure 2). Another feature of the end-members is the presence of smaller secondary modes that usually plot at the same position as the primary modes of other end-members. For example, the fine silt end-member for the modern lake samples has a secondary mode roughly centred at 150 μm that corresponds with the fine sand end-member (Figure 2). These features are likely artefacts of the EMMA (Dietze et al., 2014).

For all three datasets, the end-member loadings (Figure 2) illustrate a clear un-mixing of grain-size distributions. The end-members have broad distributions that grade into one another, but for each dataset the modeled end-members cover a unique grain-size range and mode. The EMMA models explained 85%, 86% and 66% in the Modern Lake, Danny's Lake and Carleton Lake datasets, respectively. EMMA identified five robust end-members in the Modern Lake dataset (modes: 5, 17, 63, 161 and 1822 μm), four robust end-members in the Danny's Lake dataset (modes: 5, 30, 53, 177 μm) and two robust end-members in the Carleton Lake dataset (modes: 7, 76 μm). In the modern lakes dataset the fine, coarse and very coarse silt end-members each explained a similar amount of grain-size variability and together accounted for 80% of the explained variance (Table 4). For the Danny's Lake dataset, the fine silt and the very coarse silt end-members accounted for 88.5% of the explained variance in the Danny's Lake dataset (Table 4). All three datasets contained a fine silt robust end-member (mode = 5.1 – 7.4

μm) (Figure 2 & Table 4). This provides confidence that there was minimal loss of fine grains using the Ekman grab sampling method as we see similar fine grain end-members in the freeze core records that are not susceptible to this potential sampling bias. The modern lake samples and the Danny's Lake dataset contained coarse silt (mode = 17.18 – 30.1 μm), very coarse silt (mode = 52.6 – 63.4 μm) and a fine sand (mode = 161.2 – 179.9 μm) robust end-members (Figure 2 & Table 4). The distribution of the very fine sand end-member in Carleton Lake has a wide flat peak that overlaps the same modal ranges as the very coarse silt and fine sand end-members in the Danny's Lake and modern lakes datasets, respectively. The congruency of observed robust end-members in the lake sediment cores provides confidence that similar deposition conditions are captured in the modern lakes dataset and that information from the fifty-five modern lake samples could be used to characterise the depositional conditions of end-members in the sediment cores.

Table 3. Input and boundary parameters for similarly-likely end-member model runs for robust end-member (rEM) calculation and optimal EMMA. L_{max} and L_{opt} refer to maximum and optimal weight quantiles; Q_{opt} indicates the optimal number of end-members; see Dietze et al., (2012).

Site/core	**No. of Samples**	**No. of Non-zero Grain size Classes**	**L_{max}**	**L_{opt}**	**No. of included models**	**No. of rEM**	**Total R^2 mean**	**Q_{opt}**
Modern samples	55	92	0.027	0.017	200	5	0.849	5
Danny's Lake	558	85	0	0	90	4	0.860	4
Carleton Lake	169	74	0.01	0	50	3	0.659	2

[insert Figure 2]

Figure 2. Modelled robust end-members for the modern lake samples, Danny's Lake and Carleton Lake. EMMA was based on the measured grain-size distributions (top row). Mean and one standard deviation are plotted for the robust end-members.

Table 4. Modelled robust end-members. Grain-size descriptions are based on the grain-size scale of Blott and Pye, (2001).

Dataset	Mode (µm)	Variance Explained (%)	Description
Modern samples	5.61	24.16	Fine silt
	17.18	24.99	Coarse silt
	63.42	30.85	Very coarse silt
	161.18	10.53	Fine sand
	1821.89	9.46	Very coarse sand
		0.01	
Danny's Lake	5.11	38.95	Fine silt
	30.07	9.65	Coarse silt
	52.62	49.56	Very coarse silt
	176.94	1.70	Fine Sand
		0.14	
Carleton Lake	7.42	52.24	Fine silt
	76.42	45.76	Very fine sand
		2.00	

Constrained ordination of modern lake end-members

We used a redundancy analysis to characterise depositional settings of the modern lakes (Figure 3). The environmental parameters (depth-slope, distance from shore, watershed:lake area, C:N, bottom water dissolved oxygen) explained 10.4% of the variance in the modern lake robust end-member dataset. Most of the explained variance was constrained by depth-slope (3.6%) and C:N (2.6%; Appendix 4).

[insert Figure 3]

Figure 3. Results of the redundancy analysis are shown as a correlation biplot of axes 1 and 2. Modern lake robust end-member scores were constrained by five lake environmental parameters (Table 2). Angles between and amongst response (end-members) and explanatory variables (parameters) reflect correlations. rEM – robust end-member; F, C, V – fine, coarse, very; Si, Sa – silt, sand.

We observed that sites were spread along a gradient (Figure 3). At one extreme were lakes with positive values of the depth-slope parameter – inferred to represent steep catchment and basin morphology – and negative C:N values. The other extreme consisted of lakes with negative depth-slope values – inferred to represent shallow catchment and basin morphology – and high C:N values. Danny's Lake and the very coarse silt end-member were associated with this extreme. Carleton Lake plotted towards the middle of the gradient. The coarse silt end-member was not well-constrained (short distance from origin) and plotted orthogonally to the gradient. The fine and coarse sand end-members plotted orthogonal to the gradient but in the opposite direction of the coarse silt end-member and were associated with very few sites that plotted far from the main gradient.

Stratigraphic variability of end-members

Danny's Lake. Stratigraphic variability of the robust end-members observed in the Danny's Lake core is shown in Figure 4. The base of the Danny's Lake core (*c.* 8000-7000 yr BP) is made up of the two fine-grained end-members (fine and coarse silt). This interval is coeval with low relative abundances of *Picea sp.* pollen, elevated microscopic charcoal abundances, higher $\delta^{13}C$ values and low deposition times. The distinct colour change observed at *c.* 6500 yr BP in the Danny's Lake core (Macumber et al., 2012) corresponds with the disappearance of the fine silt end-member and an increase in the very coarse silt end-member composition. The very coarse silt end-member is present prior to the colour change but only as discrete peaks, while following the colour change it becomes the dominant (0.5 – 1.0) end-member. From *c.* 6300 to 2000 yr BP only the coarse and very coarse silt end-members are present. This transition is coeval with increases in the relative abundances of *Picea sp.* pollen, decreases in microscopic charcoal abundances, lower $\delta^{13}C$ values, increases in the C:N values and elevated deposition times. From *c.* 1500-300 yr BP we observed both an increase in abundance (0.1 to 0.4) and regularity of fine sand end-member. This is coeval with decreases in relative abundances of *Picea glauca* pollen, and reduced deposition times. From *c.* 300 to -60 yr BP the fine sand end-member disappears from the record corresponding with decreases in C:N values and increases in deposition time.

[insert Figure 4]

Figure 4. Summary figure including stacked profiles of robust end-member fractional abundances in the Danny's Lake and Carleton Lake cores. Middle & Late

Holocene are defined according to (Walker et al., 2012). See discussion for definitions of climate periods and timings. Black stars represent timings of glacial advances see discussion for references. *Picea* pollen record for Danny's Lake (Sulphur et al., 2016), microscopic charcoal record for Danny's Lake (Sulphur et al., 2016), carbon and nitrogen isotope record for Danny's Lake (Griffith and Clark, 2013), chironomid inferred summer temperature reconstructions (Upiter et al., 2014). Max treeline – treeline reaches its maximum northern extent (Wolfe et al., 1996); RWP – Roman Warm Period; DAC – Dark Ages Cold Period; LIA – Little Ice Age; rEM – robust end-member; FSa – fine sand; VCSi – very coarse silt; CSi – coarse silt; FSi – fine silt; VFSa – very fine sand.

Carleton Lake. The stratigraphic variability of the robust end-members in the Carleton Lake core can be broken into four parts (Figure 4). From *c.* 2500-1500 yr BP both end-members display high amplitude variations in their abundances. Starting at *c.*1500 yr BP the very fine sand end-member is reduced in abundance and at several intervals the core consists of only the coarse silt end-member. This is coeval with lower deposition times and cooler reconstructed summer temperatures. This pattern continues until *c.*1000 yr BP when the very fine sand end-member increases in abundance, with both end-members varying in their abundances at a reduced amplitude as compared to the pattern seen from *c.* 2500-1500 yr BP. At *c.* 300 yr BP the very fine sand end-member disappears from the record and the core contains only the coarse silt end-member till present. This corresponded with increased deposition times and reconstructed summer temperatures.

Discussion

Using EMMA, we modeled robust end-members that explained most of the variance in each of the grain size datasets (Figure 2 and Table 3). The end-members identified in Danny's and Carleton Lake sediment cores were similar in their distributions to those found in the modern lakes dataset (Figure 2). From the constrained ordination of the modern lakes EMMA results we observed that sites were spread along a gradient explained by sediment C:N content and catchment-basin morphology (Figure 3). Carleton lake plotted midway along the gradient (Figure 3). Danny's Lake plotted with sites that had greater C:N values and inferred to have shallow catchment-basin morphologies. The very coarse silt end-member was also associated with these sites (Figure 3). A positive association between the very coarse silt end-member and C:N values was also observed in the Danny's Lake sediment core (Figure 4). The end-member profiles in the lake cores were highly variable and changes in their abundances were coeval with changes in other environmental proxies (Figure 4).

Depositional character of end-members

We inferred that the gradient present in the constrained ordination represented basin and catchment morphology (Figure 3). Sites with shallow catchment slopes tended to only deepen further from shore, while sites with steep catchment slopes tended to deepen closer to shore. We hypothesis that the negative association of the very coarse silt end-member with depth and shore slope could reflect that sites with shallow inclines would likely facilitate ponding of melt water: a necessary feature for the movement of coarser grains during cooler spring melts (Cockburn and Lamoureux, 2008a). This could also explain the positive association with sediment C:N values – observed both in the modern lakes and the Danny's Lake sediment core – as sites with greater values of C:N are inferred to receive a higher amount of terrestrially derived organics versus organics produced within the lake (Leng and Marshall, 2004). Since the majority of terrestrial runoff is generated during the snowmelt (Spence and Woo, 2008) we infer that the positive correlation between the very coarse silt end-member and C:N values signifies that both are likely the product of the spring melt. Future research could target other sites that plot close to Danny's Lake and evaluate their ability to track hydroclimatic variability.

The coarse silt end-member was not well-constrained by the RDA, apparent from the short distance from the origin (Figure 3). This could reflect that the coarse silt end-member is relatively abundant at all sites and does not plot strongly with any subset of sites. It's mode of 17 μm is similar to the low-energy sediment delivery regime (10-20 μm) associated with warm spring snowmelts and the finer grains deposited through much of the remaining season (Cockburn and Lamoureux, 2008b). Thus, the coarse silt end-member could represent a baseline depositional product seen throughout the year and across lake type.

Establishment of modern hydroclimate conditions (Danny's Lake)

In the central Northwest Territories, the hydraulic energy of spring runoff is modulated by the amount of winter precipitation (i.e. snowpack) and the ambient temperature (Cockburn and Lamoureux, 2008a, 2008b; Spence and Woo, 2008). Cool snowmelt conditions are characterised by an energetic delivery regime capable of bringing coarser sediment to the sample sites due to greater and longer sustained runoff (Cockburn and Lamoureux, 2008b). In contrast, warm spring conditions are characterised by low-energy delivery of more uniform finer sediment (10-20 μm) due to greater losses to ablation, infiltration and fragmentation of the snowpack (Cockburn and Lamoureux, 2008b).

The fine-grained sedimentary record prior to the colour change (*c.* 8000 to 7100 yr BP) observed in the Danny's Lake sediment core could be the result of warmer spring snowmelt conditions associated with a dryer (i.e. smaller snowpack) and hotter (i.e. warm springs) climate. Warmer and dryer conditions are inferred from: 1) elevated microscopic charcoal values in the Danny's Lake core likely reflecting increased forest fires (Sulphur et al., 2016); enrichment of $\delta^{13}C_{org}$ (Griffith and Clark, 2013) probably the result of a strong evaporation regime; and 2) low C:N values (Griffith and Clark, 2013) and relatively high abundances of green alga (Sulphur et al., 2016) that suggest warm summer temperatures promoted lake productivity. The modes of the end-member mixture (fine to coarse silt) range from

5 – 30 μm similar to the low-energy sediment (10-20 μm) observed by Cockburn and Lamoureux, (2008b), which were deposited during warm spring snowmelt.

In southern Canada the period between 7500-6000 ka has been characterised as the Early Hypsithermal (i.e., Holocene Climate Optimum) a period of warm and dry climatic conditions (Edwards et al., 1996). In addition to warmer and dryer temperatures, Edwards et al., (1996) inferred that there was a greater amount of total annual precipitation falling during the summer than during the winter with a ratio of 65:35, as compared to the modern-day summer to winter precipitation ratio of 55:45 (Edwards et al., 1996). This would have resulted in smaller snowpack. Up until 6000 yr BP, a higher cloud base enhanced the efficiency of moisture transport from the Pacific basin through the western Cordillera mountains (Edwards et al., 1996). This process would have been more pronounced during the summer resulting in a greater proportion of annual rainfall falling during summer as compared to present (Edwards et al., 1996). The hydrologic energy of summer rainfall events would have been hindered by greater evaporative losses and increased infiltration as the Danny's lake catchment was most likely free of permafrost (MacDonald and Case, 2000; Zoltai, 1995). Under these conditions only fine grains would be eroded to Danny's Lake, and indeed the grain-size range is much finer than that observed during warm spring melts by Cockburn and Lamoureux, (2008b).

The most significant sedimentological feature in the Danny's lake sedimentary record is a colour change from *c.* 7000 to 6200 yr BP. The colour change coincides with a coarsening trend in the end-member composition from a mixture of fine-grained end-members (fine and coarse silt) to a mixture of coarse and very coarse silt with the fine silt end-member disappearing from the record by *c.* 6200 yr BP. In only fifty years (*c.* 6330 to 6280 yr BP) the very coarse silt end-member increased from an average fractional abundance of 0.3 to 0.7 (Figure 4). Significant sedimentological changes have been observed in other lake proxy records and are inferred to reflect the initiation of the Holocene Thermal Maximum, a period of warm and moist climatic conditions. The timing for this transition has been roughly constrained between 6500-6000 ka (Huang et al., 2004; Kaufman et al., 2004). Our high-resolution record demonstrates that significant and persistent hydrological changes were relatively rapid (sub-centennial) based on changes in the abundance of the very coarse silt end-member (Figure 4).

Coarsening trends in lake sedimentological records can often reflect a lowering of lake water levels and an increased proximity of the core site to the shoreline. As the Holocene Thermal Maximum was characterised by an increase in moisture, a lowering of lake water levels was most likely not the cause of the coarsening trend. In the ordination of the modern lake EMMA results the very coarse silt end-member was correlated with sites further from shore (Figure 3). Thus, the very coarse silt end-member is probably not simply a product of shoreline proximity. Its association with high C:N values in both the modern lakes and Danny's lake record could reflect that this end-member is the product of terrestrial erosion. The coarsening trend is coeval with a change from a 65:35 ratio between summer and winter precipitation to the modern day ratio of 55:45 (Edwards et al., 1996). This would have increased the snowpack for spring melt resulting in coarser grains being eroded into Danny's Lake. Thus, the colour change and change in the sedimentary pattern likely represents a persistent increase in the melt energy available during the spring melt because of a hydroclimatological shift to increased wintertime precipitation. This has implications for the use of a constant reservoir correction in radiocarbon dating, as the prevailing assumption amongst researchers has been that hydrologic conditions remained constant (Patterson et al., 2017). This further increases the uncertainty of dates prior to the colour change.

Hydroclimatic changes were coincident with changes in vegetation in the Danny's Lake catchment with an overall increase in the relative abundance of *Picea mariana* pollen, interpreted as a transition from birch-shrub to spruce forest tundra community (Figure 4; Sulphur et al., 2016). From *c.* 8000 to 5000 yr BP the end-members showed a relatively large amplitude of variation with fractional abundances ranging from 1 to 0.5 (average of 0.78 ± 0.18) as compared to the sedimentary pattern following *c.* 5000 yr BP (Figure 4). This pattern of high amplitude variation is also seen in the Carleton Lake sedimentological record, with high amplitude alternations in the fine silt and very fine sand end-members from *c.* 2800-1500 yr BP (Figure 4). Although these intervals do not coincide in time they do share similar vegetation density/type within their catchments, both having low density tundra shrub type vegetation. Dense terrestrial vegetation can baffle against the action of wind in the redistribution of snow, creating deeper snowpack. In addition, dense terrestrial vegetation can stabilise soils reducing erosion and can also lead to greater losses of hydraulic energy to infiltration during summer months.

Neoglacial hydroclimate variability (Danny's & Carleton Lake)

The Neoglacial (*c.* 4300 yr BP) (Kaufman et al., 2009; Wanner et al., 2011) was a period marked by a gradual cooling trend in the central NWT (Upiter et al., 2014) with increases in annual precipitation and glacier re-advances elsewhere (Figure 4; Kaufman et al., 2009; Miller et al., 2010). We contrast the sedimentary records during relatively cool periods against relatively warmer periods during the Neoglacial for both lakes.

Several major hydrological differences exist between Danny's and Carleton Lake: 1) Carleton Lake has a larger catchment area (1.8x) that would draw more detrital material; 2) the sparse tundra shrub cover at Carleton Lake compared to dense boreal forest cover at Danny's Lake could result in less stabilization of soil; and 3) continuous permafrost present in the Carleton Lake catchment would result in less hydrologic energy loss due to infiltration. These features could explain the higher deposition times observed at Danny's Lake as compared to Carleton Lake (Figure 4).

Cooler conditions at boreal lakes are characterised by energetic delivery regimes capable of bringing coarser sediment to the sample sites due to greater and longer sustained runoff associated with reduced snow cover losses and increased ponding of meltwater (Cockburn and Lamoureux, 2008a, 2008b). In the Danny's Lake sedimentological record, the Neoglacial is characterised by a reduction in the amplitude of fluctuations in coarse and very coarse silt end-members, with the very coarse silt end-member being the most abundant (mean = 8; Figure 4). This was coeval with an increase in total *Picea* pollen relative abundances, stable $\delta^{13}C$ values, a further elevation in C:N values, and persistently reduced amounts of microscopic charcoal (Figure 4). In the modern lakes dataset, the very coarse silt end-member was correlated with sites having relatively high C:N values probably representing its relationship with terrestrial erosion, primarily derived during the spring snowmelt (Figure 3). A decreasing trend in deposition times (Figure 4) further supports that cooling and increased precipitation resulted in greater terrestrial erosion.

A further coarsening of the Danny's Lake sedimentological record corresponded with Dark Age Cold Period (*c.* 1500-1100 yr BP) (Kaufman et al., 2009; Wanner et al., 2011) and the global-scale Little Ice Age (*c.* 750-200 yr BP) (Miller et al., 2010; Wanner et al., 2011). The Dark Age Cold Period and the Little Ice Age were intervals of further cooling due to decreases in solar forcing that altered global ocean-atmospheric circulation and in the case of the Little Ice Age this was also an interval of increased tropical volcanic eruptions (Kaufman et al., 2009; Lund et al., 2006; Miller et al., 2010, 2012; Wanner et al., 2011). The appearance of the coarsest end-member in the Danny's Lake sedimentological record (*c.* 1400 yr BP) and a decreasing trend in the average fractional abundances of the coarse silt end-member was coincident with the onset of the Dark Age Cold Period. Deposition times reached their lowest values (~4 yr/mm) possibly related to increased hydraulic energy available during spring melts and the degradation of vegetation in the catchment due to climate deterioration. Prior periods of lower deposition times in the Danny's Lake sediment core corresponded with tundra shrub vegetation (*c.* 8000-7500 yr BP; Sulphur et al., 2016). The relatively greater abundance of a fine-grained end-member in the Danny's Lake sedimentary record during the Little Ice

Age agrees with Upiter et al., (2014) that in the central NWT the Dark Age Cold Period may have been a colder period than during the Little Ice Age. Increased cooling could also result in the expansion of permafrost. During the Dark Age Cold Period *Picea glauca* pollen decreased in abundance in the Danny's Lake record between *c.* 1600-1150 yr BP and all but disappears from the Danny's Lake record between *c.* 1150-900 yr BP (Figure 4; Sulphur et al., 2016). Distribution of *Picea glauca* communities is thought to be restricted to permafrost-free areas and reduced in areas of extensive permafrost (Dingman and Koutz, 1974; Sulphur et al., 2016). Permafrost expansion would have resulted in a reduction of soil infiltration during the spring melt, effectively increasing hydrologic energy.

As opposed to the Danny's Lake record, the sedimentary pattern in the Carleton Lake core is characterised by an increase in the fine silt end-member during the Dark Age Cold Period (Figure 4). This pattern persists until average chironomid reconstructed temperatures begin to rise again (Upiter et al., 2014). Very cold conditions at Carleton Lake could have resulted in perennial ice cover or short melt seasons, except this would not explain the lowered deposition times observed during this period. By this time, the treeline had already receded further south of

Carleton Lake representing the boundary of the Polar Front (Figure 4). It is possible that Carleton Lake experienced different atmospheric conditions, potentially a lowering in moisture availability resulting in reduced snowpack as opposed to conditions at Danny's Lake. Climate deterioration would have still resulted in deterioration of the vegetation in the catchment associated with greater amounts of terrestrial erosion and continuous permafrost would have limited losses due to infiltration resulting in only low energy delivery regimes being present during both spring melt and the summer months. During the Little Ice Age, deposition times are much higher and the very fine sand end-member is present in greater relative abundance. The relatively warmer temperatures during the Little Ice Age (Upiter et al., 2014) could have provided increased moisture availability for larger snowpack able to move coarser grains during spring melt.

We observed a similar sedimentary pattern in the Danny's Lake sedimentary record during Neoglacial warm periods - the fine-grained end-members increased while coarse-grained end-members decreased – as we observed during the early Middle Holocene (*c.* 8000-7500) warming periods. The increase in abundance of the coarse silt end-member at *c.* 900 yr BP and the decrease in abundance and eventual disappearance of the fine sand end-member until *c.* 800 yr BP is coeval with a warm period known as the Medieval Climate Anomaly (*c.* 1000 – 750 yr BP) (Mann et al., 2009). Chironomid-inferred mean July air temperatures at Carleton Lake were as high as 11.5°C, similar to those seen during the early Middle Holocene (Upiter et al., 2014). Longer ice-free seasons would have resulted in a greater portion of the Danny's Lake record being influenced by summer rainfall events, reduction in snow accumulation and extended melt seasons. Increases in *P. glauca* pollen during this interval could reflect degradation of permafrost that would result in greater loss of hydrologic energy to infiltration (Dingman and Koutz, 1974; Sulphur et al., 2016).

Starting at *c.* 300 yr BP the sandy end-members (Danny – fine sand; Carleton – very fine sand) all but disappeared from both records, and fine-grained end-members (Danny – coarse silt; Carleton – fine silt) continue to increase in abundance until present. C:N values, which began to decrease during the Little Ice Age, stabilize at levels not seen since the Middle Holocene (*c.* 7900 yr BP) when the central Northwest Territories was much warmer and drier. Chironomid-inferred July air temperature at Carleton Lake has increased to 12-13°C, approaching or exceeding early Middle Holocene temperatures (Upiter et al., 2014). The beginning of this interval (*c.* 300 +/- 100 yr BP) is consistent with the pre-industrial interval proposed by Hawkins et al. (2016) of 230-150 yr BP and thus the disappearance of the coarse-grained end-members in both records could represent the impacts of anthropogenic warming on spring melt conditions.

The last *c.* 300 years in the Carleton Lake sedimentological record represents unique hydroclimatical conditions as compared to the previous *c*. 3000 years, as inferred from the disappearance of the very fine sand end-member and the increase in deposition times (yr/mm). It is interesting to note that the observed pattern in deposition times closely matches that seen in the temperature reconstructions (Figure 4). The sedimentary pattern seen at Danny's Lake is similar to that observed during the early Neoglacial prior to periods of increased cooling (e.g. Dark Age Cool Period). This could highlight the greater sensitivity of more northern lakes but it also emphasises the value of longer sedimentary records in contextualising these current trends.

Evaluation of high-resolution subsampling of non-varved sediment

Both sediment cores typify lakes in the Canadian Subarctic that are characterised by very slow deposition times (yr/mm) (Crann et al., 2015). Both cores were mostly massive in texture, which could be due to high organic content of the sediment or the presence of benthic communities of organisms that might lead to mixing of the sediment. Based on our results, non-varved sediments can provide valuable proxy records, as rather than the signal being lost due to bioturbation it is only partially attenuated. The preservation of high resolution proxy data (low signal attenuation) phenomenon has been well-documented in coastal marine systems where bioturbation rates are very high when compared against those in fresh-water lake systems (e.g., Martin, 1999; Matisoff, 1982). Conventional subsampling (e.g., 0.5 cm) of our sedimentary records would result in a temporal resolution of 10 – 50 yr, while our high-resolution subsampling (Macumber et al., 2011) increased the temporal resolution to 5 – 10 yr. High-resolution subsampling better characterised the onset of the colour change in the Danny’s Lake core, showing that it was relatively rapid: taking place in approximately 50 years (Figure 4).

Conclusions

The combination of millimetre subsampling of freeze cores (Macumber et al., 2011), laser diffraction particle size analysis and EMMA has yielded valuable palaeohydroclimatologic time series of the northern treeline region. The results track both large shifts in regional hydrology as well as subtle shifts related to known climate periods. In addition, current warming trends can be placed into a millennial context to better understand their significance and target past analogue periods.

Our high-resolution records demonstrate that a major rapid hydroclimatic change took place in in the Middle Holocene (*c.* 6330-6280 yr BP) when winter precipitation increased, resulting in the spring melt becoming the major contributor of sediment to Danny's Lake. This was coeval with changes in the forest community: highlighting a potential analogue to the projected northward treeline migration under current climate trends. The relatively stable variability of Danny's Lake sedimentological record during the Neoglacial signifies that modern hydroclimate conditions have persisted for the last *c.* 6000 years and that it is a valuable record for further analyses to characterise the structure of natural hydroclimate variability in the central Northwest Territories, with implications for other treeline regions in the northern hemisphere.

Acknowledgements

This research was funded by a Natural Sciences and Engineering Research Council of Canada (NSERC) Strategic Project Grant to RTP and a Cumulative Impact and Monitoring Program – Government of the Northwest Territories grain to JMG and HF. Direct and additional funding was also provided by a NSERC Doctoral Scholarship to AM and a NSERC Visiting Fellowship to JMG, the Polar Continental Shelf Program, Carleton University, the Northwest Territories Geological Survey, the Tibbitt to Contwoyto Winter Road Joint Venture (TCWRJV), the Department of Aboriginal Affairs and Northern Development Canada, the Geological Survey of Canada, the North Slave Métis Alliance (NSMA), the Geological Society of America, Dr. George A Jeletzky Memorial Fund, the Ontario Government, the Society of Sedimentary Geology, the David and Rachel Epstein Foundation and GAC-MAC. A special thank you to Elizabeth Anderson for her valuable insight and review of the manuscript. We are especially grateful to Robert Mercredi (NSMA), Shantal Goldsmith (University of Calgary), and Lisa Neville

(Carleton University), for assistance in the sample collection and to the team of the TCWRJV (Eric Madsen, Ron Near, Donald Cockburn, Albert Brandl, Doug Nesbit, Brett Wildman, Keith White, Allan Mischuk, Terry Sharun, Kirk Keller, Ryan Lepine, Dallas Bridges and Shaun Tone). This work was carried out under Aurora Research Institute License Nos. 14435 and 14965. This manuscript represents ESS contribution number: (pending).

References

Abbott MB and Stafford TW (1996) Radiocarbon Geochemistry of Modern and Ancient Arctic Lake Systems, Baffin Island, Canada. *Quaternary Research* 45(3): 300–311.

Bianchi GG and McCave IN (1999) Holocene periodicity in North Atlantic climate and deep-ocean flow south of Iceland. *Nature* 397: 546–517.

Birks HJB, Lotter AF, Juggins S, et al. (2012) *Tracking Environmental Change Using Lake Sediments. Volume 5: Data Handling and Numerical Techniques*. *Developments in Paleoenvironmental Research*.

Blaauw M (2010) Methods and code for ‘classical’ age-modelling of radiocarbon sequences. *Quaternary Geochronology*, Elsevier B.V 5(5): 512–518.

Blaauw M and Christen JA (2011) Flexible Paleoclimate Age-Depth Models Using an Autoregressive Gamma Process. *Bayesian Analysis* 6(3): 457–474.

Blais JM and Kalff J (1995) The influence of lake morphometry on sediment focusing. *Limnol. Oceanogr.* 40(3): 582–588.

Blott SJ and Pye K (2001) GRADISTAT: a grain size distribution and statistics package for the analysis of unconsolidated sediments. *Earth Surface Processes and Landforms* 26(11): 1237–1248.

Box GE and Cox DR (1964) An analysis of transformations. *Journal of the Royal Statistical Society Series B (Methodological)*: 211–252.

Bronk Ramsey C (2009a) Bayesian analysis of radiocarbon dates. *Radiocarbon* 51(1): 337–360.

Bronk Ramsey C (2009b) Dealing with outliers and offsets in radiocarbon dating. *Radiocarbon* 51(1): 1023–1045.

Chen JA, Wan G, Zhang DD, et al. (2004) Environmental records of lacustrine sediments in different time scales: Sediment grain size as an example. *Science in China Series D* 47(10): 954–960.

Christen JA (1994) Bayesian interpretation of radiocarbon results. University of Nottingham.

Cockburn JMH and Lamoureux SF (2008a) Hydroclimate controls over seasonal sediment yield in two adjacent High Arctic watersheds. *Hydrological Processes* 22(12): 2013–2027.

Cockburn JMH and Lamoureux SF (2008b) Inflow and lake controls on short-term mass accumulation and sedimentary particle size in a High Arctic lake: implications for interpreting varved lacustrine sedimentary records. *Journal of Paleolimnology* 40(3): 923–942.

Conroy JL, Overpeck JT, Cole JE, et al. (2008) Holocene changes in eastern tropical Pacific climate inferred from a Galápagos lake sediment record. *Quaternary Science Reviews* 27(11–12): 1166–1180.

Crann CA, Patterson RT, Macumber AL, et al. (2015) Sediment accumulation rates in subarctic lakes: insights into age-depth modeling from 22 dated lake records from the Northwest Territories, Canada. *Quaternary Geochronology* 27: 131–144.

Dietze E, Hartmann K, Diekmann B, et al. (2012) An end-member algorithm for deciphering modern detrital processes from lake sediments of Lake Donggi Cona, NE Tibetan Plateau, China. *Sedimentary Geology*, Elsevier B.V. 243–244: 169–180.

Dietze E, Maussion F, Ahlborn M, et al. (2014) Sediment transport processes across the Tibetan Plateau inferred from robust grain-size end-members in lake sediments. *Climate of the Past* 10(1): 91–106.

Dietze M and Dietze E (2013) *The R-package EMMAgeo*.

Dingman SL and Koutz FR (1974) Relations among vegetation, permafrost and potential insolation in central Alaska. *Arctic and Alpine Research* 6(1): 37–47.

Doeglas DJ (1946) Interpretation of the results of mechanical analyses. *Journal of Sedimentary Research* 16(1): 19–40.

Edwards TWD, Wolfe BB and Macdonald GM (1996) Influence of Changing Atmospheric Circulation on Precipitation d 18 O – Temperature Relations in Canada during the Holocene. *Quaternary Research* 46(3): 211–218.

Foundation OSG (2015) Geographic Resources Analysis Support System (GRASS) Software. Open Source Geospatial Foundation. Available from:

http://grass.osgeo.org.

Francus P, Raymond SB, Abbott MB, et al. (2002) Paleoclimate studies of minerogenic sediments using annually resolved textural parameters. *Geophysical Research Letters* 29(20): 1998–2001.

Francus P, Bradley RS, Lewis T, et al. (2008) Limnological and sedimentary processes at Sawtooth Lake, Canadian High Arctic, and their influence on varve formation. *Journal of Paleolimnology* 40(3): 963–985.

Galloway JM, Macumber AL, Patterson RT, et al. (2010) *NWT Open Report 2010-002: Paleoclimatological Assessment of the Southern Northwest Territories and Implications for the Long-Term Viability of the Tibbitt to Contwoyto Winter Road , Part I : Core Collection*. Yellowknife, Northwest Territories, Canada.

Gauthier S, Bernier P, Kuuluvainen T, et al. (2015) Boreal forest health and global change. *Science* 349: 819–822.

Griffith F and Clark ID (2013) Holocene and recent paleoclimate investigations using carbon and nitrogen isotopes from bulk sediment of two subarctic lakes, central Northwest Territories. University of Ottawa.

Hawkins E, Ortega P, Schurer A, et al. (2016) Estimating changes in global temperature since the pre-industrial period. *Bulletin of the American Meteorological Society*.

Huang CC, MacDonald GM and Cwynar L (2004) Holocene landscape development and climatic change in the low arctic, Northwest Territories, Canada. *Palaeogeography, Palaeoclimatology, Palaeoecology* 205(3–4): 221–234.

IJmker J, Stauch G, Dietze E, et al. (2012) Characterisation of transport processes and sedimentary deposits by statistical end-member mixing analysis of terrestrial sediments in the Donggi Cona lake catchment, NE Tibetan Plateau. *Sedimentary Geology*, Elsevier B.V. 281: 166–179.

Kaufman DS, Ager TA, Anderson NJ, et al. (2004) Holocene thermal maximum in the western Arctic (0–180°W). *Quaternary Science Reviews* 23(5–6): 529–560.

Kaufman DS, Schneider DP, McKay NP, et al. (2009) Recent warming reverses long-term arctic cooling. *Science (New York, N.Y.)* 325(5945): 1236–9.

Kirby ME, Lund SP, Patterson WP, et al. (2010) A Holocene record of Pacific Decadal Oscillation (PDO)-related hydrologic variability in Southern California (Lake Elsinore, CA). *Journal of Paleolimnology* 44(3): 819–839.

Kokfelt U, Rosen P, Schoning K, et al. (2009) Ecosystem responses to increased precipitation and permafrost decay in subarctic Sweden inferred from peat and lake sediments. *Global Change Biology* 15: 1652–1663.

Leng MJ, Lamb AL, Heaton THE, et al. (2006) Isotopes in Lake Sediments. In: Leng MJ (ed.), *Isotopes in Palaeoenvironmental Research*, Netherlands: Springer, pp. 147–184.

Lund DC, Lynch-Stieglitz J and Curry WB (2006) Gulf Stream density structure and transport during the past millennium. *Nature* 444(7119): 601–604.

MacDonald GM, Edwards TWD, Moser KA, et al. (1993) Rapid response of treeline vegetation and lakes to past climate warming. *Nature* 361: 243–246.

MacDonald GM, Porinchu DF, Rolland N, et al. (2009) Paleolimnological evidence of the response of the central Canadian treeline zone to radiative forcing and hemispheric patterns of temperature change over the past 2000 years. *Journal of Paleolimnology* 41(1): 129–141.

Macumber AL, Patterson RT, Neville LA, et al. (2011) A sledge microtome for high resolution subsampling of freeze cores. *Journal of Paleolimnology* 45(2): 307–310. Available from: http://www.springerlink.com/index/10.1007/s10933-010-9487-4 (accessed 2 February 2012).

Macumber AL, Neville LA, Galloway JM, et al. (2012) *NWT Open Report 2011-010: Paleoclimatological assessment of the Northwest Territories and implications for the long-term viability of the Tibbitt to Contwoyto Winter Road , Part II : March 2010 field season results*. *NWT Open R*, Yellowknife.

Mann ME, Zhang Z, Rutherford S, et al. (2009) Global signatures and dynamical origins of the Little Ice Age and Medieval Climate Anomaly. *Science* 326(5957): 1256–1260.

Mielko C and Woo M (2006) Snowmelt runoff processes in a headwater lake and its catchment, subarctic Canadian Shield. *Hydrological Processes* 20(4): 987–

1000.

Miller GH, Brigham-Grette J, Alley RB, et al. (2010) Temperature and precipitation history of the Arctic. *Quaternary Science Reviews*, Elsevier Ltd 29(15–16): 1679–1715.

Miller GH, Geirsdóttir Á, Zhong Y, et al. (2012) Abrupt onset of the Little Ice Age triggered by volcanism and sustained by sea-ice/ocean feedbacks. *Geophysical Research Letters* 39(2).

Moser KA and MacDonald GM (1990) Holocene Vegetation Change at Treeline North of Yellowknife, Northwest Territories, Canada. *Quaternary Research* 34(2): 227–239.

Mullan D, Swindles GT, Patterson RT, et al. (2016) Climate change and the long-term viability of the World's busiest heavy haul ice road. *Theoretical and Applied Climatology*.

Murray MR (2002) Is laser particle size determination possible for carbonate-rich lake sediments ? *Journal of Paleolimnology* 27(2): 173–183.

Natural Resources Canada (2009) *Canada-Permafrost Map*.

Natural Resources Canada (2015a) Geogratis. Available from: geogratis.cgdi.gc.ca (accessed 17 September 2015).

Natural Resources Canada (2015b) *The atlas of Canada: environment*.

Oksanen J, Blanchet F, Roeland Kindt G, et al. (2013) vegan: Community Ecology Package. Available from: http://cran.r-project.org/package=vegan.

Osborne JW (2010) Improving your data transformations : Applying the Box-Cox transformation. *Practical Assesment, Research & Evaluation* 15(12).

Patterson RT, Crann CA, Cutts JA, et al. (In Press) New occurrences of the White River Ash (east lobe) in Subarctic Canada and utility for estimating freshwater reservoir effect in lake sediment archivese. *Palaeogeography, Palaeoclimatology, Palaeoecology*.

Paul CA, Rühland KM and Smol JP (2010) Diatom-inferred climatic and environmental changes over the last ~9000years from a low Arctic (Nunavut, Canada) tundra lake. *Palaeogeography, Palaeoclimatology, Palaeoecology*, Elsevier B.V. 291(3–4): 205–216.

Pienitz R, Smol JP and Macdonald GM (1999) Paleolimnological reconstruction of Holocene climatic trends from two Boreal Treeline Lakes, Northwest Territories, Canada. *Arctic, Antarctic, and Alpine Research* 31(1): 82–93.

Rao C (1995) A review of canonical coordinates and an alternative to correspondence analysis using Hellinger distance. *Questiio* 19(1–3): 23–63.

Reimer PJ, Bard E, Bayliss A, et al. (2013) Intcal13 and marine13 radiocarbon age calibration curves 0 – 50,000 years cal bp. *RADIOCARBON* 55: 1869–1887.

Rühland KM and Smol JP (2005) Diatom shifts as evidence for recent Subarctic warming in a remote tundra lake, NWT, Canada. *Palaeogeography, Palaeoclimatology, Palaeoecology* 226(1–2): 1–16.

Smith SL, Wolfe SA, Riseborough DW, et al. (2009) Active-Layer Characteristics and Summer Climatic Indices, Mackenzie Valley, Northwest Territories, Canada. *Permafrost and Periglacial Processes* 20(2): 201–220.

Spence C and Woo M (2008) Hydrology and the Northwestern Canadian Shield. In: Woo M (ed.), *Cold Region Atmospheric and Hydrologic Studies. The Mackenzie GEWEX Experience. Volume 2: Hydrologic Processes*, Berlin Heidelberg New York: Springer, p. 497 pp.

Sperazza M, Moore JN and Hendrix MS (2004) High-resolution particle size analysis of naturally occurring very fine-grained sediment through laser diffractometry. *Journal of Sedimentary Petrology* 74(5): 736–743.

Sulphur KC, Goldsmith SA, Galloway JM, et al. (2016) Holocene fire regimes and treeline migration rates in sub-arctic Canada. *Global and Planetary Change* 142: 42–56.

Sun D, Bloemendal J, Rea DK, et al. (2002) Grain-size distribution function of polymodal sediments in hydraulic and aeolian environments , and numerical partitioning of the sedimentary components. *Sedimentary Geology* 152(3): 263–277.

Upiter LM, Vermaire JC, Patterson RT, et al. (2014) Middle to late Holocene chironomid-inferred July temperatures for the central Northwest Territories, Canada. *Journal of Paleolimnology* 52(1–2): 11–26.

van Hengstum PJ, Reinhardt EG, Boyce JI, et al. (2007) Changing sedimentation patterns due to historical land-use change in Frenchman's Bay, Pickering, Canada: evidence from high-resolution textural analysis. *Journal of Paleolimnology* 37(4): 603–618.

Viau AE and Gajewski K (2009) Reconstructing millennial-scale, regional paleoclimates of boreal Canada during the holocene. *Journal of Climate* 22(2): 316–330.

Walker MJC, Berkelhammer M, Bjorck S, et al. (2012) Formal subdivision of the Holocene Series / Epoch : a Discussion Paper by a Working Group of INTIMATE (Integration of ice-core , marine and terrestrial records) and the Subcommission on Quaternary Stratigraphy (International Commission on Stratigraphy . *Journal of Quaternary Science* 27(7): 649–659.

Walsh JE, Overland JE, Groisman PY, et al. (2011) Ongoing Climate Change in the Arctic. *Ambio* 40(S1): 6–16.

Wanner H, Solomina O, Grosjean M, et al. (2011) Structure and origin of Holocene cold events. *Quaternary Science Reviews*, Elsevier Ltd 30(21–22): 3109–3123.

Wanner H, Mercolli L, Grosjean M, et al. (2015) Holocene climate variability and change; a data-based review. *Journal of the Geological Society* 172: 254–263.

Weltje GJ and Prins MA (2003) Muddled or mixed? Inferring palaeoclimate from size distributions of deep-sea clastics. *Sedimentary Geology* 162(1–2): 39–62.

Weltje GJ and Prins MA (2007) Genetically meaningful decomposition of grain-size distributions. *Sedimentary Geology* 202(3): 409–424.

Wolfe BB, Edwards TWD, Aravena R, et al. (1996) Rapid Holocene hydrologic change along boreal tree- line revealed by (delta) 13C and (delta) 180 in organic lake sediments, Northwest Territories, Canada. *Journal of Paleolimnology* 15(2): 171–181.

Xiao J, Chang Z, Fan J, et al. (2012) The link between grain-size components and depositional processes in a modern clastic lake. *Sedimentology* 59(3): 1050–1062.

Zoltai SC (1995) Permafrost distribution in peatlands of west-central Canada during the Holocene warm period 6000 years BP. *Geographie Physique Et Quaternaire* 49(1): 45–54.

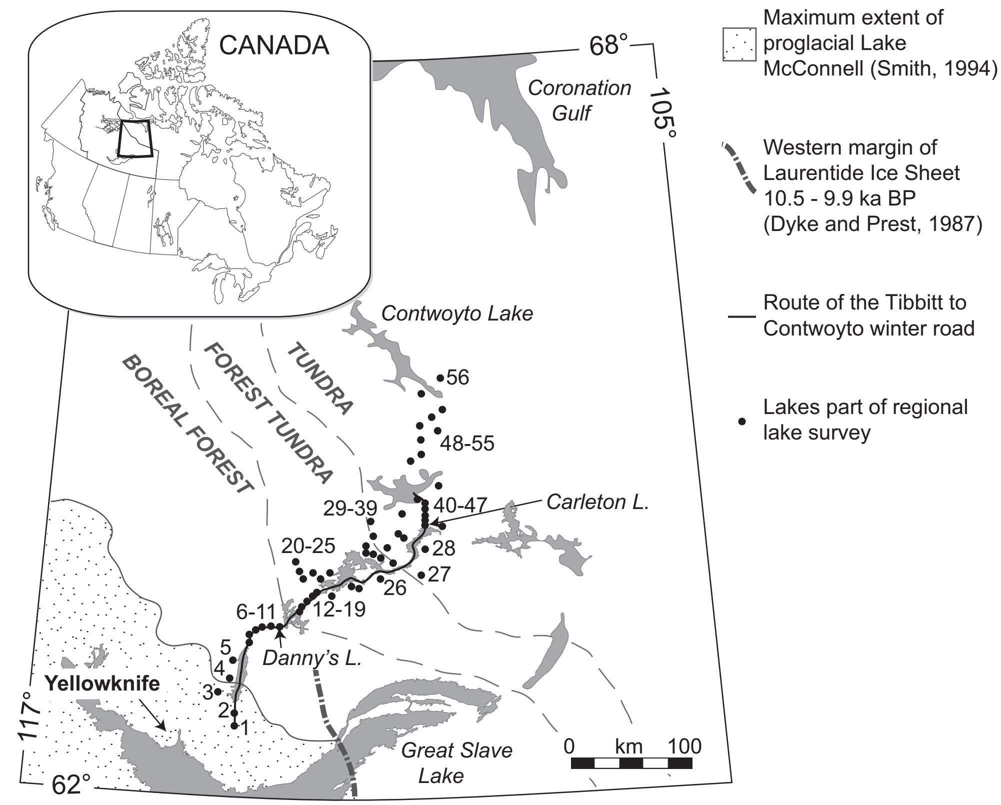
CANADA
68°
105°
117°
62°
Coronation Gulf
Contwoyto Lake
TUNDRA
FOREST TUNDRA
BOREAL FOREST
Carleton L.
Danny's L.
Yellowknife
Great Slave Lake
0 km 100
56
48-55
40-47
29-39
20-25
28
27
26
12-19
6-11
5
4
3
2
1
Maximum extent of proglacial Lake McConnell (Smith, 1994)
Western margin of Laurentide Ice Sheet 10.5 - 9.9 ka BP (Dyke and Prest, 1987)
Route of the Tibbitt to Contwoyto winter road
Lakes part of regional lake survey

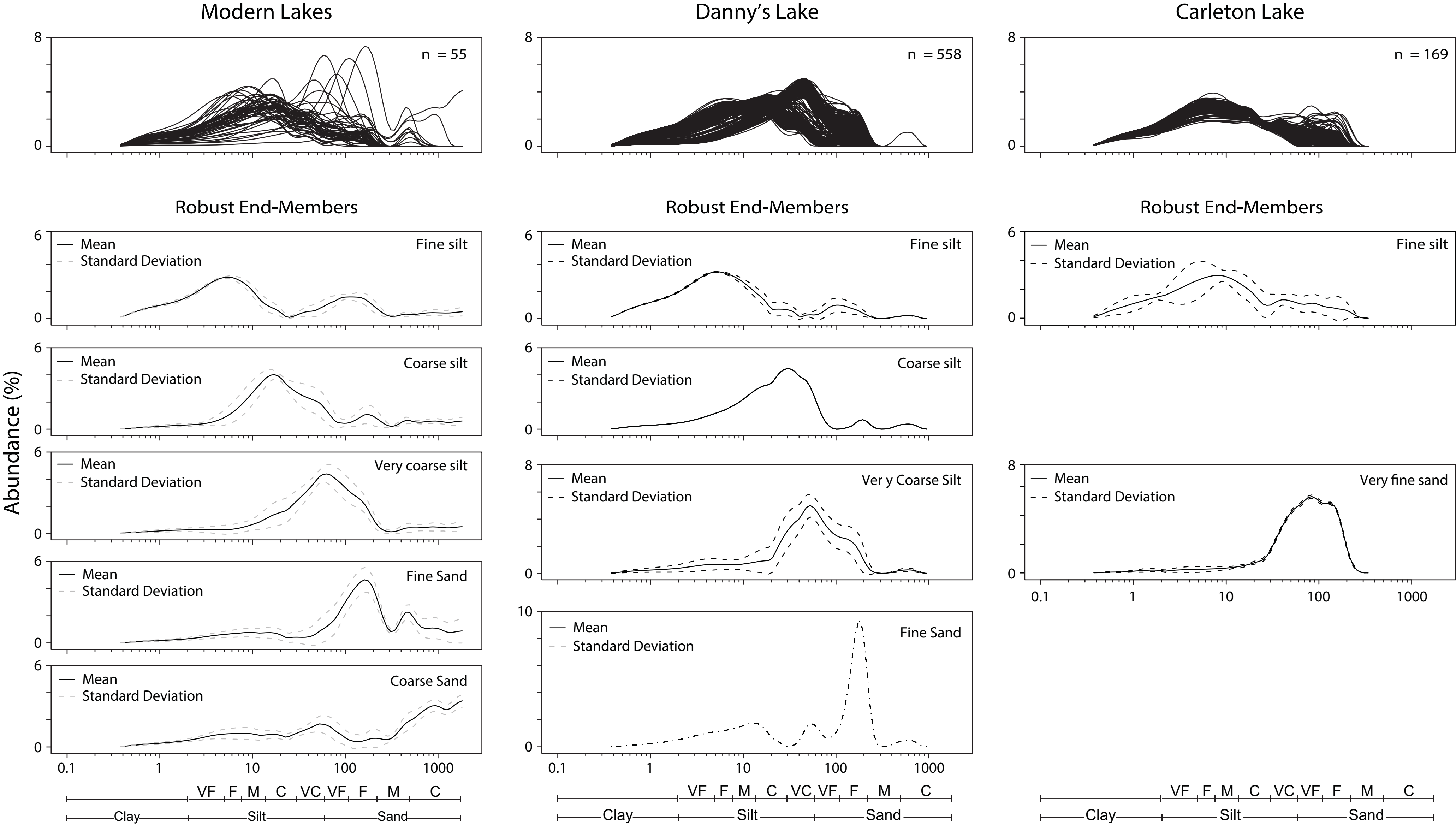

Modern Lakes
Danny's Lake
Carleton Lake
n = 55
n = 558
n = 169
Robust End-Members
Robust End-Members
Robust End-Members
Mean
Standard Deviation
Fine silt
Coarse silt
Very coarse silt
Fine Sand
Coarse Sand
Ver y Coarse Silt
Very fine sand
Abundance (%)
0.1
1
10
100
1000
VF F M C VC VF F M C
Clay
Silt
Sand

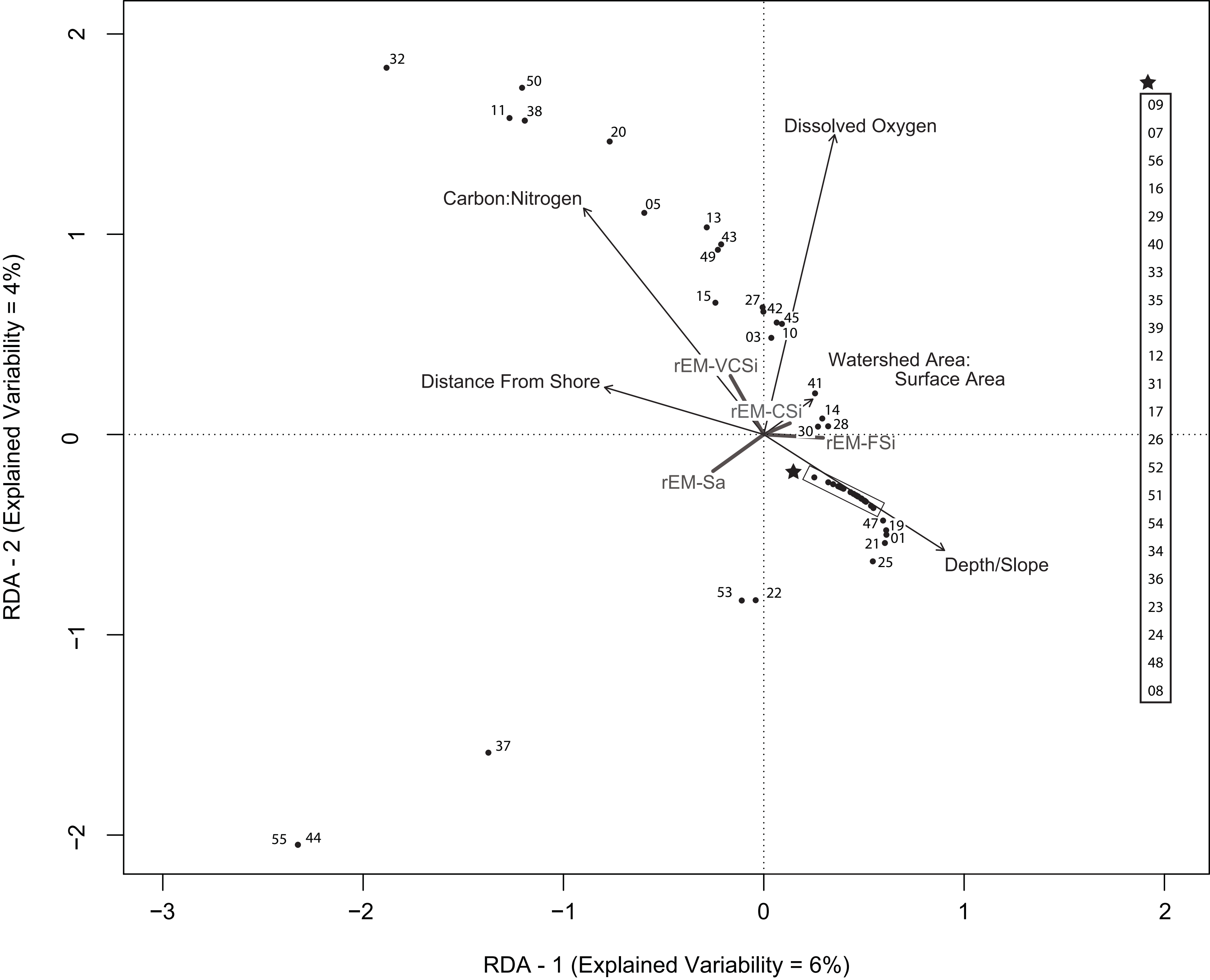

RDA - 2 (Explained Variability = 4%)
RDA - 1 (Explained Variability = 6%)
Dissolved Oxygen
Carbon:Nitrogen
Watershed Area:
Surface Area
Distance From Shore
Depth/Slope
rEM-VCSi
rEM-CSi
rEM-FSi
rEM-Sa
32
50
11
38
20
05
13
43
49
15
27
42
45
03
10
41
14
28
30
47
19
01
21
25
53
22
37
55
44
09
07
56
16
29
40
33
35
39
12
31
17
26
52
51
54
34
36
23
24
48
08

Sequence	Field Code	Lake Name	Latitude DD	Longitude DD	Depth m	Surface Area (SA) m^2	Shore Distance m	Shore Slope degrees	Watershed Area (WA) m^2	WA:SA ratio	DO %	C:N ratio
11	R11-18-006	Danny's	63.4773	-112.5406	4.0	208286	110	2.70	836494	4.02	63.20	9.92
41	R11-13-006	Carleton	64.2586	-110.0987	1.9	312599	180	2.75	1522313	4.87	83.70	11.33
1	R11-17-002	Dome	62.7707	-113.2579	6.0	2907380	60	6.20	3378282	1.16	6.70	9.53
2	R11-17-001	Waite	62.8493	-113.3313	2.0	*	50	4.10	*	*	53.90	*
3	R11-17-003		62.9532	-113.4521	5.0	1187483	60	6.30	3254828	2.74	86.40	12.10
4	R11-17-004		63.0154	-113.3049	8.0	92381	50	8.40	426066	4.61	1.80	*
5	R11-17-005		63.1354	-113.2303	6.0	109462	50	9.80	268170	2.45	32.00	15.27
6	R11-17-006		63.3185	-113.0742	3.0	93596	60	6.90	347815	3.72	91.10	*
7	R11-17-007		63.3918	-112.8742	7.2	1148580	80	16.10	2606462	2.27	26.70	8.49
8	R11-18-003		63.4009	-112.8503	5.5	230127	30	8.50	1033980	4.49	71.40	10.42
9	R11-18-004	Pat's	63.4174	-112.6931	6.1	459362	80	8.65	918675	2.00	76.20	10.45
10	R11-18-005		63.4584	-112.5538	3.8	604897	50	3.15	1781234	2.94	91.10	11.92
12	R11-18-007		63.5171	-112.3143	11.0	366725	60	10.30	1899573	5.18	1.70	12.74
13	R11-18-008		63.5869	-112.3057	2.0	363817	130	2.40	2121714	5.83	92.10	11.47
14	R11-18-009		63.5935	-112.2944	1.5	129119	90	2.60	1433298	11.10	92.50	19.26
15	R11-18-010		63.6005	-112.2977	1.2	91220	110	3.50	306518	3.36	91.90	22.29
16	R11-18-011		63.6589	-111.9747	4.8	360667	110	3.50	1164102	3.23	91.60	9.12
17	R11-15-006		63.6764	-111.6016	5.9	92893	60	4.95	460995	4.96	69.10	12.39
18	R11-15-005		63.7402	-111.2879	4.0	10814294	160	2.45	2112873	0.20	94.10	12.64
19	R11-15-004		63.7419	-111.2239	4.0	2079913	60	2.80	7339397	3.53	88.90	10.67
20	R11-19-003		63.7590	-112.2072	2.3	1116690	160	6.10	1994634	1.79	97.20	12.72
21	R11-18-012		63.7605	-111.8213	3.0	60313	50	3.70	966668	16.03	89.40	10.43
22	R11-19-004		63.7883	-112.2990	1.5	266375	100	3.00	778039	2.92	96.80	12.82
23	R11-19-005		63.7995	-112.3226	2.0	247333	130	2.95	1014500	4.10	83.50	13.33
24	R11-19-002		63.7997	-111.9859	2.0	184849	130	1.70	508415	2.75	97.20	13.83
26	R11-15-003		63.8110	-110.8762	3.6	409253	80	4.90	1053979	2.58	88.60	13.39
25	R11-19-001		63.8164	-111.6848	2.5	282409	30	4.90	1239970	4.39	95.10	11.53
29	R11-15-002		63.8866	-110.6116	5.0	86635	40	5.60	569523	6.57	86.90	13.98
27	R11-15-001		63.9022	-110.0866	3.2	310980	90	3.15	705348	2.27	90.70	12.49
30	R11-19-011		63.9822	-110.8662	10.0	1162351	150	5.45	2956844	2.54	94.50	13.95
31	R11-19-009		63.9829	-111.1393	5.5	601308	190	3.70	1101198	1.83	93.10	12.20
32	R11-19-010		63.9880	-111.0611	3.0	365822	200	5.70	933787	2.55	95.10	14.46
33	R11-19-008		64.0043	-111.1423	6.5	1597846	340	1.90	2652457	1.66	94.80	14.37
34	R11-19-012		64.0327	-110.8094	4.0	328249	100	7.10	1681722	5.12	94.30	12.64
28	R11-13-007	Mackay	64.0370	-110.1182	3.0	825983	200	3.72	1608449	1.95	89.80	12.00
35	R11-19-007		64.0558	-111.0597	2.0	276276	50	2.50	733222	2.65	94.40	12.85
36	R11-19-006		64.1061	-111.1059	2.0	145936	100	3.15	1210128	8.29	93.90	12.86
37	R11-19-014	Queen's	64.1251	-110.5696	4.5	462148	50	3.10	1213687	2.63	91.40	13.05
38	R11-19-013		64.1271	-110.6607	2.0	706783	180	2.20	1402115	1.98	96.80	14.01
40	R11-18-002		64.2515	-109.7730	5.0	200216	40	5.00	1091303	5.45	90.70	13.11
42	R11-13-005		64.2684	-110.0929	3.1	176441	150	5.30	775599	4.40	89.00	11.35
43	R11-13-004	Horseshoe	64.2898	-110.0604	3.9	5503466	120	2.55	8559486	1.56	92.20	11.98
39	R11-18-001		64.2939	-110.4167	3.5	553824	130	2.90	2364404	4.27	33.20	12.02
44	R11-13-002	Abe	64.4121	-110.1000	2.4	2634928	180	3.50	4955017	1.88	67.80	10.84
45	R11-13-003	Echo	64.4195	-110.1053	7.0	2634928	120	7.50	4955017	1.88	85.70	10.98
46	R11-14-011	Lac de Gras	64.4302	-110.1364	9.0	*	200	2.50	*	*	101.80	10.16
47	R11-14-010		64.4989	-109.9538	7.1	2247502	250	8.65	3398477	1.51	98.40	10.75
48	R11-14-009		64.6499	-110.2748	8.0	1154158	170	2.90	2036197	1.76	90.50	11.67
49	R11-14-008		64.7201	-109.9979	2.8	271635	100	2.30	968145	3.56	95.30	12.33
50	R11-14-007		64.8395	-110.0559	4.5	110016	120	1.90	454172	4.13	98.00	12.25
51	R11-14-006		64.9244	-110.1353	6.5	2300407	340	5.20	3810561	1.66	71.00	11.87
52	R11-14-005		64.9499	-109.6473	7.2	1151438	310	1.20	2299681	2.00	93.00	14.24
53	R11-14-004		65.0642	-109.9141	6.0	992500	220	2.20	1538769	1.55	92.20	12.25
54	R11-14-003		65.1404	-109.8022	3.2	537264	300	1.90	2118495	3.94	96.70	8.39
55	R11-14-002		65.2584	-110.0904	4.4	1149299	190	2.90	4129985	3.59	23.50	12.41
56	R11-14-001		65.3834	-109.8228	3.5	1116457	300	6.90	993662	0.89	93.00	8.79